Atomic-Scale Mechanisms of the Glass-Forming Ability in Metallic Glasses

L. Yang, G. Q. Guo, L. Y. Chen, C. L. Huang, T. Ge, D. Chen, P. K. Liaw, K. Saksl, Y. Ren, Q. S. Zeng, B. LaQua, F. G. Chen, and J. Z. Jiang

Phys. Rev. Lett. **109**, 105502 — Published 7 September 2012

DOI: 10.1103/PhysRevLett.109.105502

Atomic-scale mechanisms of the glass-forming ability in metallic glasses

L. Yang[1,a)], G. Q. Guo**[1], L. Y. Chen[2], C. L. Huang[1], T. Ge[1], D. Chen[1], P. K. Liaw[3], K. Saksl[4], Y. Ren[5], Q. S. Zeng[6], B. LaQua[7], F. G. Chen[1], and J. Z. Jiang[2,a)],

[1]College of Materials Science and Technology, Nanjing University of Aeronautics and Astronautics, Nanjing 210016, P.R. China

[2]International Center for New-Structured Materials (ICNSM), Zhejiang University and Laboratory of New-Structured Materials, Department of Materials Science and Engineering，Zhejiang University, Hangzhou 310027, P.R. China

[3]Department of Materials Science and Engineering, The University of Tennessee, Knoxville, TN 37996 USA

[4]Institute of Materials Research, Slovak Academy of Sciences, Watsonova 47, 04001 Kosice, Slovakia

[5]Advanced Photon Source, X-ray Science Division, Argonne National Laboratory, Argonne, IL 60439 USA

[6]Department of Geological & Environmental Sciences, Stanford University, Stanford, CA 94305-2115 USA

[7]Department of Materials Science and Engineering, University of Wisconsin-Madison, Madison, WI 53706 USA

a) Authors to whom correspondence should be addressed: electronic mail: yangliang@nuaa.edu.cn and jiangjz@zju.edu.cn

** Contributes equally with the first author.

PACS: 61.05.cj, 61.05.cp, 61.43.Dq, 61.43.Bn

Abstract

The issue, composition dependence of glass-forming ability (GFA) in metallic glasses (MG), has been investigated by systematic experimental measurements coupled with theoretical calculations in Cu-Zr and Ni-Nb alloy systems. It is found that the atomic-level packing efficiency strongly relates to their GFA. The best GFA is located at the largest difference in the packing efficiency of the solute-centered clusters between the glassy and crystal alloys in both MG systems. This work provides an understanding of GFA from atomic level and will shed light on the development of new MGs with larger critical sizes.

Since the discovery of the first glassy alloy with the composition of $Au_{75}Si_{25}$ in 1960[1], vast efforts have been devoted to understanding the mechanisms for glass formation in metals. Numerous rules, criteria, and mechanisms have been proposed to guide the development of metallic alloys with high glass-forming ability (GFA)[2-6]. Recent experimental studies show that the best glass former in an alloy system is located at a pinpoint composition[7-9]. The existing mechanisms and criteria for glass formation fail to explain why the best glass former only occurs at a pinpoint composition. Recently, Li et al. found that the best glass former corresponds to a distinct peak in the mass density of the amorphous phase[10]. However, the cause of the distinct density maxima of the amorphous phase is still unknown. Here, this issue will be addressed from the aspect of the atomic-level microstructure.

The atomic-level microstructure of metallic glasses (MGs) is a long-standing subject that has been attracting large interest[11-16]. Although the atomic structural picture is far from being established, it has been realized that clusters should be the building block in glassy alloys. Therefore, these clusters may be the key for understanding MG microstructures. Many structural models have been proposed by studying the clusters theoretically or experimentally. Early models include the hard-sphere random-packing model[17] and stereochemically designed model[18].Recently, more efficient models were developed, such as the cluster packing model[19] and quasi-equivalent clusters model[20]. These models enhance the understanding of the glass-forming mechanisms in MGs by building and packing clusters topologically and chemically to reveal their short-range and medium-range

ordering. However, the dependence of the relatively high GFA on the atomic-level microstructure in the pinpoint bulk MG compositions is still far from being understood. It has been suggested in previous work[21,22] that clusters in these pinpoint compositions have similarly indexed topological and chemical characters compared to those in neighboring compositions. Thus, it is difficult to explicitly reveal the origin of GFA subtly tuned by compositions in alloy systems only by studying the indexed characters of clusters obtained from these structural models. Accordingly, new ideas are required to address this issue.

In this work, a feasible scheme for understanding the cause of the density maxima of the amorphous phase was developed by calculating the atomic packing efficiencies inside the clusters and the regularity of these building blocks based on synchrotron radiation experiments in MGs. The CuZr alloy system was selected as the research prototype in this work because it has: 1) a broad composition region forming MG ribbons[23]; 2) several identified compositions for forming bulk MGs[9,24,25]; 3) a relatively simple system, enhancing the reliability of structural results[26]. Cu_xZr_{100-x} (x = 61.8, 63, 64, 64.5, and 65.5 at.%) alloys were chosen and studied in this paper because they cover one of the eutectic points ($Cu_{61.8}Zr_{38.2}$) and one of the previously identified bulk MG compositions ($Cu_{64}Zr_{36}$). Zr atoms are regarded as the solutes due to their concentration. This meets the stoichiometric demand of the solute-centered cluster structural model[19,20].

The alloy ingots were prepared by arc melting the mixture of Zr [99.9wt.%] and Cu [99.9wt.%] elements in Ti-gettered high-purity argon atmosphere The ingots were

melted at least 4 times in order to ensure their compositional homogeneity. The corresponding amorphous ribbons were fabricated by melt-spinning[27], producing a cross section of 0.04 × 2 mm^2. The synchrotron radiation-based high-energy (about 100 keV) X-ray diffraction measurements were performed for all samples at the beam line, BW5, of Hasylab in Germany. The two-dimensional diffraction data were recorded using a Mar345 image plate. Subsequently, using the transmission mode, Zr and Cu K-edge extended X-ray absorption fine structure (EXAFS) spectra were measured at the beam lines, A1, in Hasylab, and BL14W1, in the Shanghai Synchrotron Radiation Facility of China. The diffraction patterns and EXAFS spectra were normalized via a standard data-reduced procedure[27], employing the software PDFgetX[28] and Visual Processing in EXAFS Researches (VIPER)[29], respectively. In order to obtain the atomic structural information as reliably as possible, both the normalized diffraction and EXAFS data were simulated simultaneously under the framework of reverse Monte-Carlo (RMC)[20,30]. Cubic boxes that we used in the RMC simulation contained 40,000 atoms, matching the Cu_xZr_{100-x} (x = 61.8, 63, 64, 64.5, and 65.5) compositions. Additionally, the simulated atomic structural models were further analyzed by the Voronoi tessellation method[20,31].

Figs. 1(a)-(d) show the total pair distribution function, G(r), the structural factor, S(Q) (obtained from the diffraction measurements), and the Zr, Cu K-edge EXAFS data in the CuZr alloys, along with their corresponding simulated curves. The good matching confirms the reliability of the RMC simulation. The atomic structural data, including the first-shell coordination numbers and the atomic pair distances are listed

in Table S1. In addition, the Cu- and Zr-centered Voronoi clusters (VC) are extracted and indexed, whose distributions are plotted in Fig. S1. The data in Table S1 changes monotonously and gently with the compositional variation and the VCs distributions in Fig. S1 are very similar among the five CuZr MGs, representing no unique structural character in the $Cu_{64}Zr_{36}$ bulk MG. These results indicate that the dependence of the GFA on the microstructure in the CuZr alloy system cannot be explained only by the information deduced above.

It has been suggested that the dense packing principle may be the key factor for GFA[19,32], but this has not been verified yet. Therefore, a scheme was designed for calculating the atomic-level packing efficiency to reveal their GFA. In crystallography, the packing efficiency is defined as the volume ratio of the atoms within one unit cell to the unit cell itself[33]. Based on this definition, the atomic-packing efficiency (η) inside the indexed Cu- and Zr-centered VCs was calculated by

$$\eta = \frac{V_a}{V_u} \tag{1}$$

where V_a and V_u denote the volume of the embedded atoms inside a cluster and the total volume of the cluster itself, respectively. V_u can be obtained by summing the volumes of all the VCs containing tetrahedra because each VC is built by stacking tetrahedra with a shared vertex, located at the site of the VC's center atom[34]. Because each atom embedded in the cluster is truncated as a cone ball, thus, V_a can be calculated by summing the volumes of all the cone balls. To show the feature of the clusters and its containing atoms more explicitly, a three-dimensional configuration is illustrated in Fig. 2. The atomic-packing efficiencies of Cu- and Zr-centered VCs of

all samples are plotted in Fig. 3(a). It was observed that all the η values of Zr-centered VCs are obviously larger than those of Cu-centered counterparts This is because more neighbor atoms can be more densely packed around the large center (Zr atom) than a small center (Cu atom). The intriguing phenomenon revealed in Fig. 3(a) is that the atomic-packing efficiency exhibits a local maximum at the $Cu_{64}Zr_{36}$ composition for both the Cu- and Zr-centered VCs. To compare the atomic-packing efficiency with the dependence of GFA on compositions, the GFA of the investigated compositions was quantitatively characterized by the critical casting size (the largest size for an alloy composition to obtain amorphous structure via casting method). The critical casting size of the compositions studied is listed in Table S3. It is interesting that $Cu_{64}Zr_{36}$ is one of the identified compositions with a local maximum of GFA, which suggests that there is a close correlation between the atomic-packing efficiency defined here and the GFA in glassy alloys.

To further address this issue, the atomic-packing efficiency, $\eta_{c,}$ of both Cu- and Zr-centered cluster in the hypothetical "ideal" crystal alloys were also calculated using the same compositions of the five CuZr glasses. Because all the selected CuZr MGs can transform into the mixture of Cu_8Zr_3 and $Cu_{10}Zr_7$ crystal phases[35] after crystallization, each "ideal" crystal phase should be made up of these two crystal phases according to their stoichiometric ratio. Thus η_c is calculated by

$$\eta_c = \sum_i C_i \eta_i \tag{2}$$

$$\eta_i = \frac{\sum_j X_j V_{aj}}{\sum_j X_j V_{uj}} \quad (3)$$

where C_i and η_i denote the concentration and atomic-packing efficiency of the i-th crystal component to form the "ideal" crystal, respectively. X_j is the fraction of the Cu- or Zr-centered clusters with a center atom at the j-th Wykoff site (The method to extract clusters in crystal phases refers to our previous work[36]). V_{aj} and V_{uj} represent the volume of the embedded atoms in the j-th type of clusters and the volume of the j-th type of clusters, respectively. The η_c values of Cu- and Zr-centered clusters in the "ideal" crystal alloys are compared to those of the glassy clusters, η, in Fig. 3(a). It is important to note that all the η values of Zr-centered clusters are at least 1.5% larger than those in crystal alloys, whereas in the Cu-centered clusters, the η values are at least 0.5% smaller than their η_c counterparts. Considering their elemental concentration, Zr and Cu atoms are regarded as the solutes and solvents, respectively. This indicates that the solute-centered clusters are more compact structural units than solvent-centered clusters. Therefore, solute-centered clusters should be regarded as the backbones to build the microstructures of glassy alloys, which is consistent with the concept of the solute-centered cluster structural model[19,20]. It is also important to note that there is no significant change of η_c values among these five compositions.

To further analyze the relation between the packing efficiency and GFA, $(\eta-\eta_c)/\eta_c$ are calculated and plotted in Fig. 3(b). A local maximum (3%) of the difference ratios occurs in the Zr-centered clusters for $Cu_{64}Zr_{36}$. This maximum indicates that the packing efficiency within the building blocks of this pinpoint bulk MG is extremely

high, compared with that of its corresponding crystal alloy. In other words, the local highest atomic-packing efficiency occurs at this composition and the best GFA is achieved. Furthermore, the Zr-centered major VCs in all of these CuZr MGs are not the preferred clusters contained in the corresponding crystal phases, but are the favored building blocks in glassy alloys, with abundant fivefold-rotation symmetry features[37]. They should be the cause for stabilization of the glassy state and accordingly, the stability of these VCs strongly relates to the GFA in the alloys. If the atoms in these VCs posses the highest atomic-packing efficiency in the glassy state, the VCs will be very compact and stable, making them less likely to collapse or transform during quenching into the preferred crystal VCs, resulting in high GFA. This is the structural origin of the $Cu_{64}Zr_{36}$ MG with the best GFA in the selected CuZr compositional region.

Since we have found that the distributions of Cu- and Zr-centered indexed VCs are similar in all five CuZr MGs, the question is raised, why does the local highest atomic-packing efficiency occur specifically at $Cu_{64}Zr_{36}$ bulk MG composition? It is acknowledged that the more regular a polyhedron is, the more compact it should be, such as the regular tetrahedron, the cube, and the sphere. Therefore, the regularity of the VCs in these CuZr MGs was investigated. The details of the calculation method are described in supplemental materials. The tetrahedrisity values (denoted by T, the variance of the edge lengths in a tetrahedron, which indicates its regularity)[38,39] of all the cluster-containing tetrahedra in all five samples are plotted in Fig. 4. It obviously shows that a minimum of the tetrahedrisity values occurs in the $Cu_{64}Zr_{36}$ bulk MG,

which suggests that the tetrahedra and even the VCs in this composition should possess the highest regularity. Accordingly, they are the most compact and stable building blocks in the glassy state.

In previous work, it was also proved that the local structures closest to the spherical symmetry leads to the best GFA[40,41], which coincides with our results here. By analyzing the atomic-packing efficiency at the short-range scale (within a cluster), it is found that the atomic packing efficiency in the solute-centered clusters should be higher in the glassy state than in the crystal phase. Nevertheless, because the clusters in glasses have the abundant fivefold-symmetry features and are more irregular structural units than those in crystals, they can not be connected with enough neighbors to create a long-range structural ordering. Instead, they exhibit the fractal feature at the medium-range scale, resulting in a lower cluster-level packing efficiency than that of crystals or quasicrystals, which fill the space better[42]. Therefore, at the macroscopical scale, the mass density is smaller in glasses than in the corresponding crystal alloys[43]. However, in the $Cu_{64}Zr_{36}$ bulk MG, the atoms in the solute-centered clusters are more densely packed than its crystal counterpart and the building blocks are more regular than those of its neighbor glassy compositions, so the packing efficiency is enhanced. Therefore, at the macroscopical scale, it is expected that the $Cu_{64}Zr_{36}$ bulk MG possesses a higher packing efficiency (density) than neighboring compositions, closer to its crystal counterpart. Recently, in Li's work, a method to measure the mass density in glasses was developed[10,44]. This work expressed that the difference ratio of the mass densities between a MG and its

corresponding crystal alloy reaches the local minimum at a composition with the best GFA, consistent with the results presented here.

A recent study shows that liquid structure correlates with nucleation barrier[45]. Since GFA is related to nucleation of competing crystalline phases, it is expected that there is a relationship between GAF and structure. The results in this work demonstrated this correlation. According to classical nucleation theory, nucleation is expected to exponentially change as a function of composition. An interesting future work would be to investigate whether the structure parameters studied in this work follow an exponential behavior.

A similar analysis was performed on another representative binary alloy system, NiNb, which also has a well-known bulk-metallic-glass composition at $Ni_{62}Nb_{38}$[46,47]. The detailed information is described in the supplementary file. This analysis also validates the arguments presented in this work.

Conclusion

The microstructure of CuZr alloys were investigated by calculations based on the data from synchrotron radiation-based XRD and EXAFS experiments. Although the cluster-level topological and chemical character is similar in five selected glassy alloys, a relatively high atomic-packing efficiency in the Zr (solute)-centered clusters occurs in the bulk $Cu_{64}Zr_{36}$ MG, and these compact clusters possess the local highest regularity, contributing to the stability of this glass alloy. These structural features of $Cu_{64}Zr_{36}$ MG lead to it having the best GFA of the compositions studied. This finding was also confirmed in the NiNb binary alloy system. By developing a method to

calculate the atomic-packing efficiency within clusters, this work provides a feasible scheme for investigating the dependence of GFA on the microstructure in alloys at the atomic and cluster scale, providing an in-depth understanding of the glass-forming mechanism in this class of glassy materials.

Acknowledgments

The authors would like to thank the HASYLAB in Germany, the Shanghai Synchrotron Radiation Facility in China, and the Advanced Photon Source in the United States for the use of the advanced synchrotron radiation facilities. Financial support from the National Natural Science Foundation of China (Grant No. 10805027, 10979002, 50920105101, 51071141, 51050110136, and 10904127), the Natural Science Foundation of Jiangsu Province (Grant No. BK2011071), the NUAA Research Funding (Grant No. NS2010168), the Funding for Outstanding Doctoral Dissertation in NUAA (Grant No. BCXJ12-08), the National Key Basic Research Program of China (2012CB825700), Zhejiang University-Helmholtz cooperation fund, and the fundamental research funds for the central Universities are gratefully acknowledged. PKL very much appreciates the financial support by the U.S. National Science Foundation (CMMI – 0900271, DMR – 0909037, and CMMI - 1100080) with Drs. C.V. Cooper, D. Finotello, and A. Andell as contract monitors. Karel Saksl is indebted to the Slovak Grant Agency for Science for financial support (grant No. 2/0167/10).

References

[1] W. Clement, R.H. Willens, and P. Duwez, Nature (London) **187**, 869 (1960).

[2] D. Turnbull, Contmp. Phys. **10**, 473 (1969).

[3] A.L. Greer, Nature (London) **366**, 303 (1993).

[4] A. Inoue, Acta Mater. **48**, 279 (2000).

[5] Z.P. Lu, H. Tan, Y. Li, and S.C. Ng, Scripta Mater. **42**, 667 (2000).

[6] Z.P. Lu, and C.T. Liu, Phys. Rev. Lett. **91**, 115505 (2003).

[7] D. Wang, H. Tan, and Y. Li, Acta Mater. **53**, 2969 (2005).

[8] Y. Shen, E. Ma, and J. Xu, J. Mater. Sci. Technol. **24**, 149 (2008).

[9] D. Wang, Y. Li, B.B. Sun, M.L. Sui, K. Lu, and E. Ma, Appl. Phys. Lett. **84**, 4029 (2004).

[10] Y. Li, Q. Guo, J.A. Kalb, and C.V. Thompson, Science **322**, 1816 (2008).

[11] W.H. Wang, C. Dong, and C.H. Shek, Mater. Sci. Eng. R **44**, 45 (2004).

[12] Z.P. Lu, C.T. Liu, J.R. Thompson, and W.D. Porter, Phys. Rev. Lett. **92**, 245503 (2004).

[13] W.H. Wang, Prog. Mater. Sci. **52**, 540 (2007).

[14] D.B. Miracle, D.V. Louzguine-Luzgin, L.V. Louzguina-Luzgina, and A. Inoue, Int. Mater. Rev. **55**, 218 (2010).

[15] Q.S. Zeng, H.W. Sheng, D. Yang, L. Wang, W.G. Yang, J.Z. Jiang, W.L. Mao, and H.K. Mao, Science **332**, 1404 (2011).

[16] Q.K. Jiang, G.Q. Zhang, L. Yang, X.D. Wang, K. Saksl, R. Wunderlich, H. Fecht, and J.Z. Jiang, Acta Mater. **55**, 4409 (2007).

[17] J.D. Bernal, Nature (London) **183**, 141 (1959).

[18] P.H. Gaskell, Nature (London) **276**, 484 (1978).

[19] D.B. Miracle, Nature Mater. **3**, 697 (2004).

[20] H.W. Sheng, W.K. Luo, F.M. Alamgir, J.M. Bai, and E. Ma, Nature (London) **439**, 419 (2006).

[21] T. Fujita, K. Konno, W. Zhang, V. Kumar, M. Matsuura, A. Inoue, T. Sakurai, and M.W. Chen, Phys. Rev. Lett. **103**, 075502 (2009).

[22] L. Yang, G.Q. Guo, L.Y. Chen, S.H. Wei, J.Z. Jiang, and X.D. Wang, Scripta Mater. **63**, 879 (2010).

[23] A. Inoue, J. Mater. Sci. **16**, 1391 (1981).

[24] A. Inoue, and W. Zhang, Mater. Trans. **45**, 584 (2004).

[25] D.H. Xu, B. Lohwongwatana, G. Duan, W.L. Johnson, and C. Garland, Acta Mater. **52**, 2621 (2004).

[26] X.D. Wang, S. Yin, Q.P. Cao, J.Z. Jiang, H. Franz, and Z.H. Jin, Appl. Phys. Lett. **92**, 011902 (2008).

[27] L. Yang, G.Q. Guo, G.Q. Zhang, and L.Y. Chen, J. Mater. Res. **25**, 1701 (2010).

[28] http://www.pa.msu.edu/cmp/billinge-group/programs/PDFgetX/.

[29] http://www.cells.es/Beamlines/CLAESS/software/viper.html.

[30] L. Yang, S. Yin, X.D. Wang, Q.P. Cao, J.Z. Jiang, K. Saksl, and H. Franz, J. Appl. Phys. **102**, 083512 (2007).

[31] S.Y. Wang, M.J. Kramer, M. Xu, S. Wu, S.G. Hao, D.J. Sordelet, K.M. Ho, and C.Z. Wang, Phys. Rev. B **79**, 144205 (2009).

[32] A.L. Greer, and E. Ma, Mater. Res. Bull. **32**, 611 (2007).

[33] D. Schwarzenbach, Crystallography, John Wiley and Sons, Inc. (1996).

[34] N.N. Medvedev, J. Comput. Phys. **67**, 223 (1986).

[35] P. Villars, and L.D. Calvert, Pearson's Handbook of Crystallographic Data for Intermetallic Phases, American Society for Metals, Metal Park, Ohio (1985).

[36] L. Yang, J.H. Xia, Q. Wang, C. Dong, L.Y. Chen, X. Ou, J.F. Liu, J.Z. Jiang, K. Klementiev, K. Saksl, H. Franz, J.R. Schneider, and L. Gerward, Appl. Phys. Lett. **88**, 241913 (2006).

[37] L. Yang, and G.Q. Guo, Chin. Phys. B **12**, 126101 (2010).

[38] N.N. Medvedev, and Y.I. Naberukhin, J. Non-Cryst. Solids **94**, 402 (1987).

[39] A.V. Anikeenko, M.L. Gavrilova, and N.N. Medvedev, Generalized Voronoi Diagram: Structural analysis of hard sphere packing, Spinger-Verlag Berlin Heidelberg (2009).

[40] X.K. Xi, L.L. Li, B. Zhang, W.H. Wang, and Y. Wu, Phys. Rev. Lett. **99**, 095501 (2007).

[41] X.K. Xi, M.T. Sandor, Y.H. Liu, W.H. Wang, and Y. Wu, Scripta Mater. **61**, 967 (2009).

[42] D. Ma, A.D. Stoica, and X.L. Wang, Nature Mater. **8**, 30 (2009).

[43] A. Inoue, T. Negishi, H.M. Kimura, T. Zhang, and A.R. Yavari, Mater. Trans. JIM **39**, 318 (1998).

[44] Q. Guo, J.H. Noh, P.K. Liaw, P.D. Rack, Y. Li, and C.V. Thompson, Acta Mater. **58**, 3633 (2010).

[45] G.W. Lee, A.K. Gangopadhyay, T.K. Croat, T.J. Rathz, R.W. Hyers, J.R. Rogers, and K.F. Kelton, Phys. Rev. B **72**, 174107 (2005).

[46] L. Xia, W.H. Li, S.S. Fang, B.C. Wei, and Y.D. Dong, J. Appl. Phys. **99**, 026103 (2006).

[47] L.Y. Chen, H.T. Hu, G.Q. Zhang, and J.Z. Jiang, J. Alloys Compd. **443**, 109 (2006).

Figure Caption

Figure 1 (a) Total pair distribution function, G(r), (b) Structure factor, S(Q), (c) Cu K-edge, and (d) Zr K-edge EXAFS spectra. The solid and dashed lines denote experimental and simulation data, respectively. The k and $\chi(k)$ represent the photoelectron wave vector and the k-space EXAFS signal, respectively.

Figure 2 The left is a representative ideal icosahedron, the center is one of its tetrahedron components, and the right is a perspective to show the tetrahedron and its embedded atomic parts. The blue and green balls stand for the shell and center atoms of the icosahedron, respectively.

Figure 3 (a) The atomic-packing efficiencies, η, in five selected CuZr MGs and their corresponding values, η_c, in the hypothetical "ideal" crystal alloys, and (b) the difference ratio between η and η_c, i.e., $(\eta-\eta_c)/\eta_c$

Figure 4 The variance of the edge lengths. *T*, of all the tetrahedra forming the VCs in the selected five CuZr samples, which determines the regularity of tetrahedra and even the corresponding VCs.

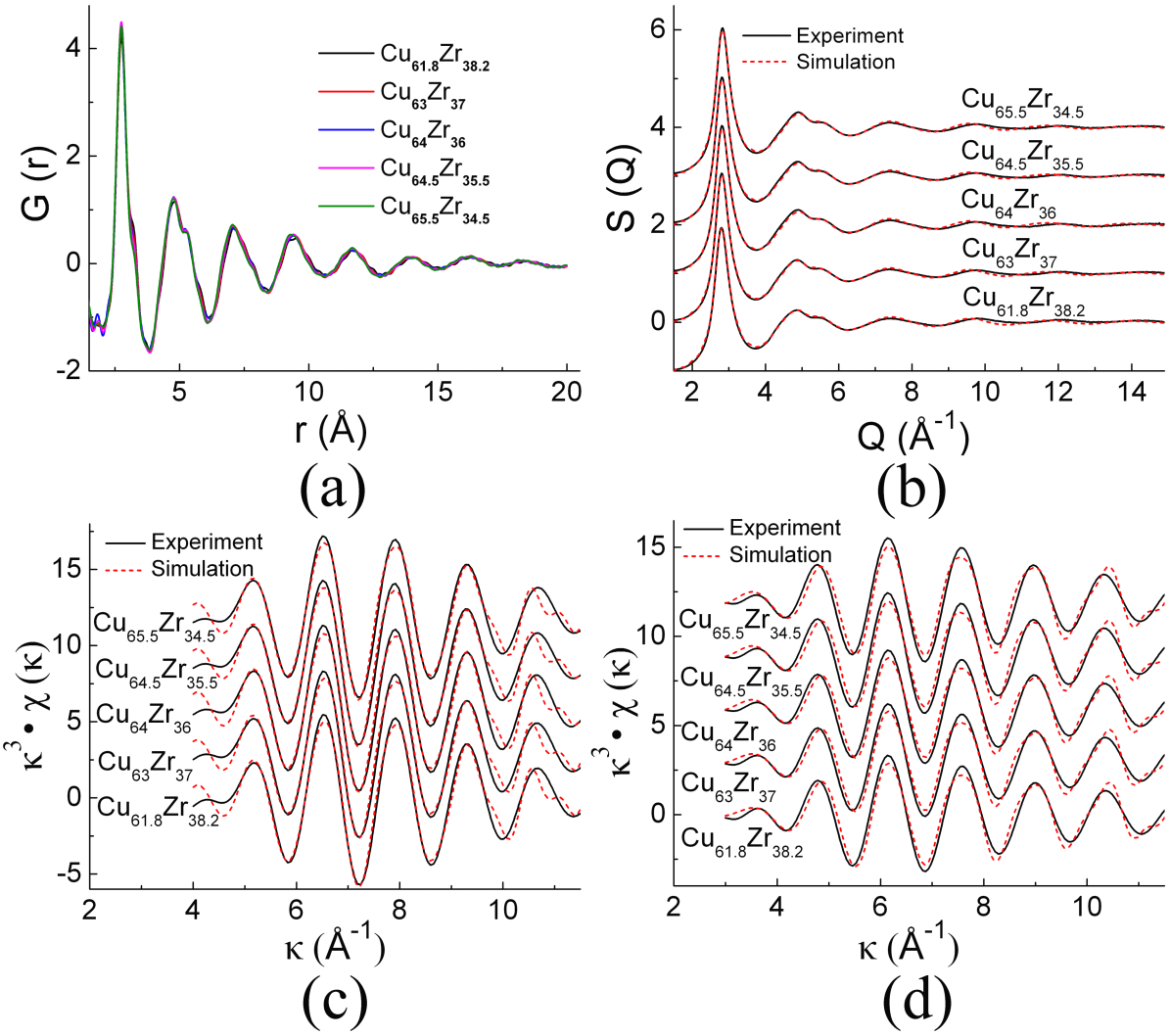
G (r)
r (Å)
Cu61.8Zr38.2
Cu63Zr37
Cu64Zr36
Cu64.5Zr35.5
Cu65.5Zr34.5
(a)
S (Q)
Q (Å-1)
Experiment
Simulation
Cu65.5Zr34.5
Cu64.5Zr35.5
Cu64Zr36
Cu63Zr37
Cu61.8Zr38.2
(b)
κ3 • χ (κ)
κ (Å-1)
Experiment
Simulation
Cu65.5Zr34.5
Cu64.5Zr35.5
Cu64Zr36
Cu63Zr37
Cu61.8Zr38.2
(c)
κ3 • χ (κ)
κ (Å-1)
Experiment
Simulation
Cu65.5Zr34.5
Cu64.5Zr35.5
Cu64Zr36
Cu63Zr37
Cu61.8Zr38.2
(d)

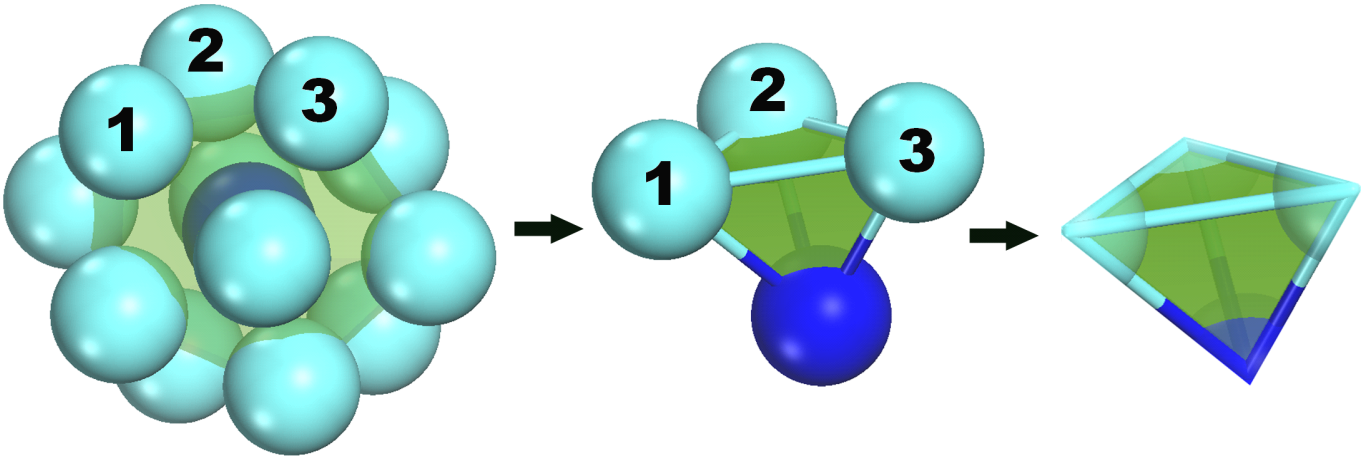
2
1
3
2
1
3

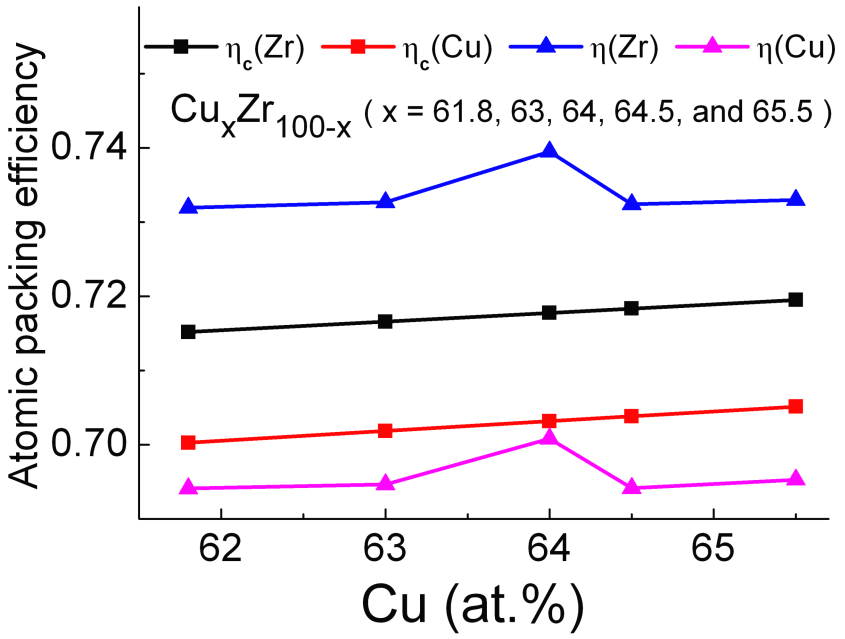
ηc(Zr)
ηc(Cu)
η(Zr)
η(Cu)
CuxZr100-x (x = 61.8, 63, 64, 64.5, and 65.5)
Atomic packing efficiency
0.74
0.72
0.70
62
63
64
65
Cu (at.%)

(a)

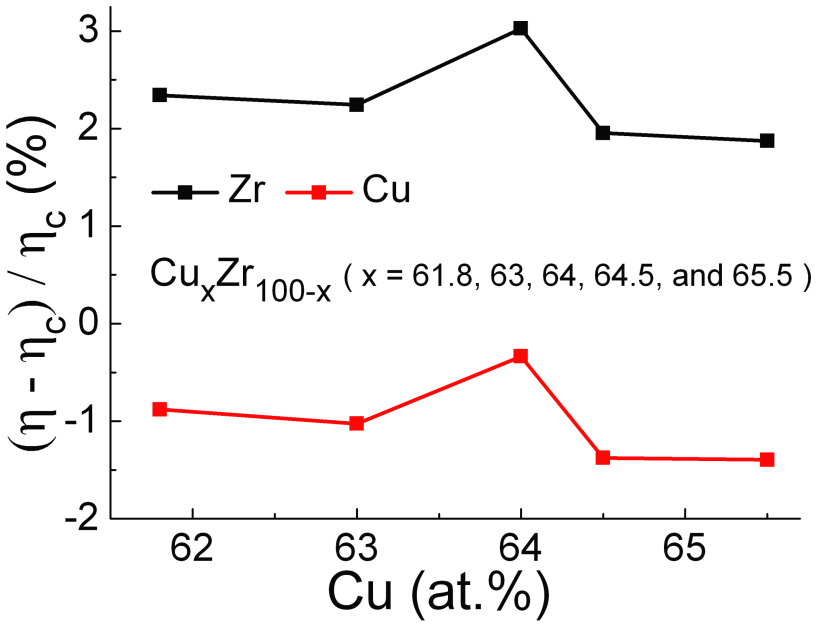
3
2
1
0
-1
-2
(η - ηc) / ηc (%)
Zr
Cu
CuxZr100-x (x = 61.8, 63, 64, 64.5, and 65.5)
62
63
64
65
Cu (at.%)

(b)

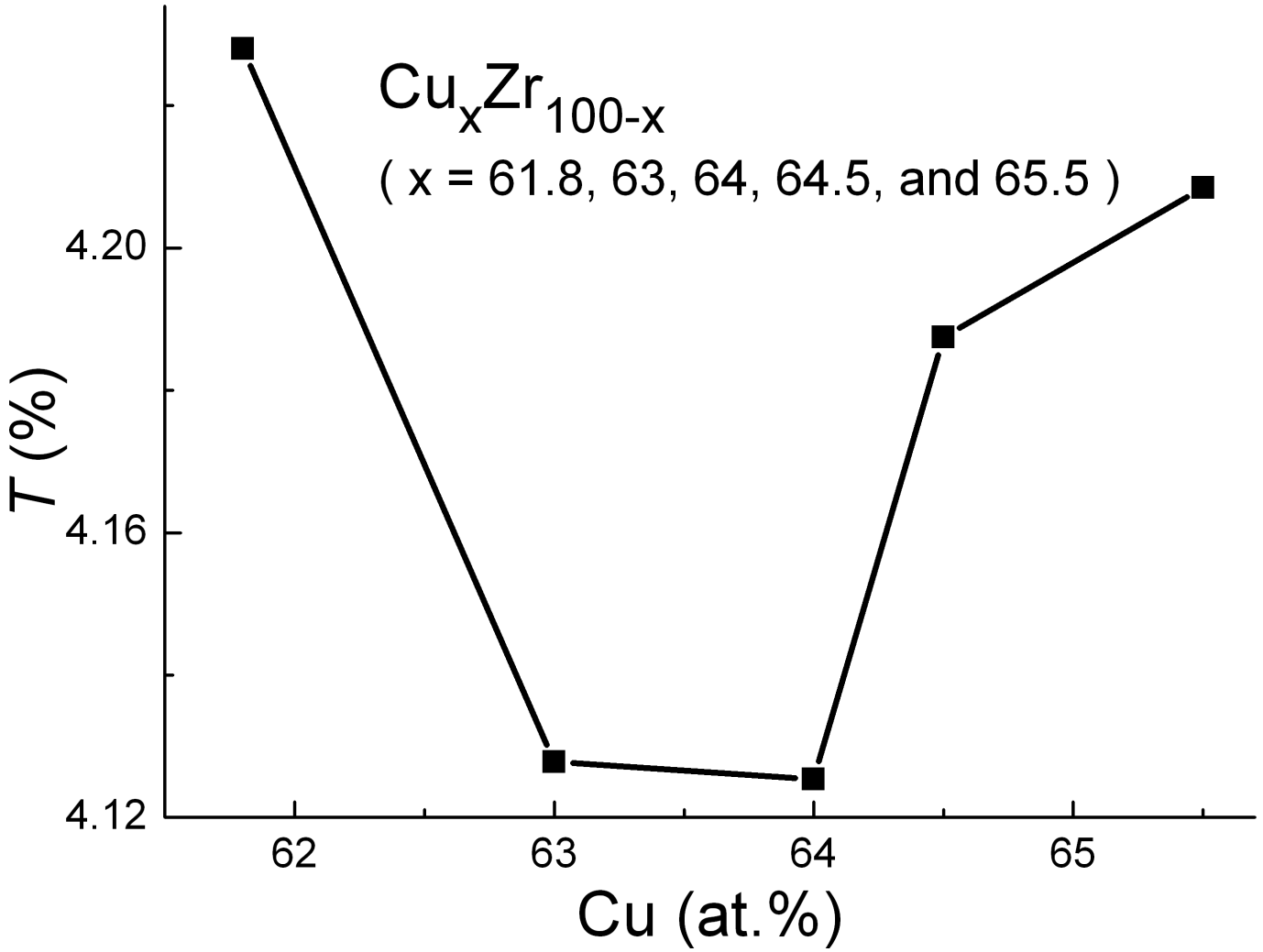
Cu$_x$Zr$_{100-x}$
(x = 61.8, 63, 64, 64.5, and 65.5)
4.20
4.16
4.12
T (%)
62
63
64
65
Cu (at.%)